Probing axial anisotropy in dinuclear alkoxide-bridged Er–COT single molecule magnets

Maximilian G. Bernbeck, Jeremy D. Hilgar, Jeffrey D. Rinehart*

University of California - San Diego, Department of Chemistry and Biochemistry, La Jolla, California, 92122, USA.

KEYWORDS (Word Style "BG_Keywords"). If you are submitting your paper to a journal that requires keywords, provide significant keywords to aid the reader in literature retrieval.

ABSTRACT: Developing well-coupled lanthanide-based magnetic materials via a building block approach has proven difficult since few systems exists that are able to simultaneously maintain anisotropy and promote adequate coupling. Employing the anisotropic building block consisting of Er^{3+} bound to the cyclooctatetraenide dianion ($[Er(COT)]^{+}$), two alkoxide-bridged dinuclear single-molecule magnets displaying ferromagnetic coupling were synthesized: centrosymmetric $[Er(COT)(\mu\text{-}OEt)]_2$ (**1**) and non-centrosymmetric $[Er(COT)(THF)](\mu\text{-}O^tBu)_2[Er(COT)]$ (**2**). AC relaxation studies reveal that both systems have similar weak temperature dependence of their relaxation, despite anisotropy axes being parallel in **1** and nearly perpendicular in **2**. Due to the strong crystal field provided by the alkoxide ligands, both complexes display enhanced mixing of the total angular momentum states, which provides a fast relaxation pathway despite conserved single-ion anisotropy and ferromagnetic coupling.

The design of discrete molecules exhibiting superparamagnetic relaxation behavior has accelerated over the past two decades.[1,2] Instead of a classical rotation of a magnetization vector traversing an energy barrier, magnetic relaxation in these single-molecule magnets (SMMs) is best described by transition probabilities between quantized states with different orientations of the molecular electron angular momentum. The energies and transition probabilities of these states are controlled by the ligand field interaction, allowing for the development of synthetic design principles toward the optimization of these properties on a molecular level. Such methods have been successfully applied to design transition metal[3–5] and lanthanide[6–9] based SMMs. Lanthanide-based SMMs, in particular, offer highly anisotropic spin-orbit coupled ground states with large moments that can be stabilized by enforcing a particular crystal field environment.[10,11] Adherence to these principles has yielded extraordinary results that outperform other SMMs in their single-ion anisotropy.[12–14]

To expand diversity and introduce collective behavior to SMMs, considerable current work is focused on synthesizing well-coupled molecular magnetic systems. This coupling can curtail the low-temperature quantum tunneling of the magnetization (QTM) mechanism of magnetic relaxation by increasing the total effective moment of the ground state in a molecular magnetic system. However, coupling in SMMs has proven incompatible with the retention of magnetic anisotropy, largely because both phenomena are generally facilitated by the same orbitals. It is difficult to construct a ligand scaffold that introduces coupling without disturbing the crystal field environment responsible for generating single-ion anisotropy within individual magnetic centers. To add further synthetic complexity, the molecular scaffold must orient the individual ions' anisotropy axes such that the net effect is non-zero and axial. While current research in using well-oriented diamagnetic bridges[15] and radical-based bridging ligands[16–20] in lanthanide systems has demonstrated that weak coupling need not be a limiting factor for multinuclear magnets, a unified set of synthetic design principles accounting for both coupling and anisotropy remain a collective challenge for the field.

One approach to directly targeting well-coupled multinuclear magnetic clusters and materials is through the bottom-up assembly of highly anisotropic synthetic building blocks.[3,21,22] Ideally, by incorporating metal centers with large inherent single-ion anisotropy into larger molecular frameworks, anisotropy in the resultant material would be conserved and enhanced *via* suitably strong ferromagnetic coupling. Inspired by examples of robust anisotropy in Er^{3+} stabilized by the strong equatorial crystal field provided by the cyclooctatetraenide dianion (COT^{2-}) described over the last decade,[21–30] we have displayed the conserved anisotropy of Er^{3+} coordinated to a single COT^{2-} ligand.[31] We employed the resultant Metal-Ligand-Pair Anisotropy (MLPA) to measure the effect of anisotropy axis collinearity on magnetic relaxation inhibition.[32] Herein we enact a more drastic modification by introducing strongly Lewis basic alkoxide bridging ligands. While the changes to the electronic structure are dramatic and complex, we can interpret them in terms of perturbations from the known electronic structure of the individual units and from the observed properties of our previously described $Er(COT)I(THF)_2$ and $[Er(COT)I(MDPP)]_2$.

Magnetic analyses are presented here for a centrosymmetric and non-centrosymmetric dinuclear Er^{3+} system bridged by simple alkoxide ligands. As they commonly form multitopic bridging interactions stabilized by charge and hard Lewis acid/base interactions, the library of multinuclear alkoxide-bridged lanthanide systems with known magnetic properties is rich.[33–42] However, most of these systems exhibit poor relaxation dynamics and often have negligible axial anisotropy, either due to strong mixing of the ground spin-orbit coupled states or the weak exchange coupling provided by the alkoxide ligands. Some systems have overcome this

`

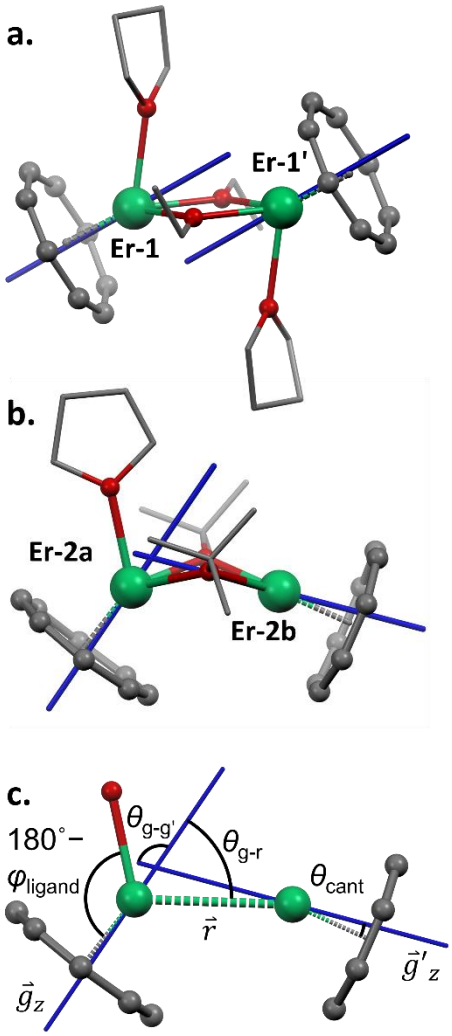

Figure 1: Solid-state structures for **1** (a) and **2** (b). Principle anisotropic axes (g_z) are shown in blue. Full structures for **1** and **2** have hydrogens omitted and non-COT carbons depicted as capped sticks for clarity. Angles and vectors are illustrated in the structure for **2**, omitting extraneous atoms for clarity (c).

by using scaffolds to enforce alignment of the principle anisotropic axes to promote ferromagnetic dinuclear coupling.[43] Here we observed consequential perturbations by hard Lewis basic alkoxide ligands to the anisotropy in two dinuclear Er^{3+} species. Despite observed ferromagnetic coupling, through-barrier relaxation mechanisms are still operant, limiting long-timescale relaxation.

Results and Discussion

Synthetic and Structural Information

Complexes **1** and **2** were synthesized using standard air- and water-free techniques by adding potassium ethoxide (KOEt) or potassium *tert*-butoxide (KO^{t}Bu), respectively, to Er(COT)I(THF)$_2$ in tetrahydrofuran (THF). After removing KI, complex **1** was crystallized from concentrated THF at −50 °C; complex **2** was crystallized *via* the slow diffusion of pentane into a concentrated THF solution at ambient temperature. No monomeric side products have been observed. Both compounds are thermodynamically stable at ambient temperatures under inert atmospheric conditions.

Solid state structures of **1** and **2** (Figures 1, S1, S2) were determined by single crystal X-ray crystallographic methods using a Mo K(α) source. Compound **1** crystallizes in the orthorhombic *P*bca space group, while compound **2** crystallizes in the orthorhombic *P*nma space group. An isomorphous structure to **1** exists for Nd,[44] while no structural analog exists for **2**.

Compound **1** has two THF-bound $[Er(COT)]^+$ units doubly bridged by μ_2-ethoxide ligands related by a crystallographically imposed inversion center. Previous investigations into the magnetism of $[Er(COT)]^+$ complexes have identified the axis containing the Er^{3+} ion and the COT^{2-} centroid ($\vec{r}_{ErCOT}$) to correlate closely to the magnetic anisotropy,[31] making it a useful crystallographic parameter to describe the crystal field environment. The COT^{2-} ligand is bound relatively far from the Er^{3+} ion at $|\vec{r}_{ErCOT,\mathbf{1}}|$= 1.82 Å, which is expected to weaken its ability to stabilize single-ion anisotropy of Er^{3+}.[45] To describe the axial or equatorial coordination of each non-COT ligand, coordination angles with respect to $\vec{r}_{ErCOT}$, defined as φ_{ligand}, were measured. In **1**, ligands are all bound above

the magic angle, with φ_{OEt} = 43.45° and 45.56° and φ_{THF} = 54.71°, suggesting a net destabilization of the m_J = 15/2 doublet.[6,10] The distance between Er^{3+} centers ($|\vec{r}_{Er-Er'}|$), 3.543 Å, is shorter than observed in iodide-bridged dinuclear [Er(COT)]$^+$ systems. As dipolar coupling strength scales proportional to $1/r^3$, we expect a stronger ferromagnetic dipolar interaction between [Er(COT)]$^+$ units. The angle between $\vec{r}_{ErCOT}$ and the Er–Er′ internuclear vector ($\vec{r}_{Er-Er'}$) was found to be $\theta_{ErCOT,\mathbf{1}\text{-r}}$ = 26.01° and is equivalent by symmetry for each erbium center.

Compound **2** has crystallographically imposed C_s symmetry and is comprised of two [Er(COT)]$^+$ units bridged by two μ_2-*tert*-butoxide ligands. Two distinct Er^{3+} coordination environments exist, Er-**2a** and Er-**2b**. Er-**2a** has φ_{OtBu} = 49.04° and φ_{THF} = 50.00° with $|\vec{r}_{ErCOT,\mathbf{2a}}|$ = 1.84 Å, while Er-**2b** has φ_{OtBu} = 37.19° with $|\vec{r}_{ErCOT,\mathbf{2b}}|$ = 1.79 Å; both centers are expected to display poor m_J = 15/2 stabilization due to their long $\vec{r}_{ErCOT}$ distances and relatively axial alkoxide and THF binding motif. The Er^{3+} centers are significantly closer together in **2** than in **1** with $|\vec{r}_{Er-Er}|$ = 3.439 Å. The two independent $\vec{r}_{ErCOT}$ vectors are also positioned significantly differently, with $\theta_{ErCOT,\mathbf{2a}\text{-r}}$ = 22.52°, $\theta_{ErCOT,\mathbf{2b}\text{-r}}$ = 53.81°, and $\theta_{ErCOT\text{-}ErCOT}$ = 103.7°.

From our previous work, we expect several of these structural parameters to be of great importance to the magnetic analysis; in particular, contrasting **1** and **2** to our previously studied dinuclear species containing the [Er(COT)]$^+$ unit illustrates key differences. First, the relative $\vec{r}_{ErCOT}$ angle ($\theta_{ErCOT\text{-}ErCOT}$) shifts from parallel in **1** to nearly perpendicular in **2** (103.71°). Our previous study on iodide-bridged materials found a marked slowing of the magnetization dynamics for more parallel angles, culminating in a 100-fold increase in the relaxation time at 2 K when changing the angle from 113° in [Er(COT)I]$_2$(DPPM) to 180° in [Er(COT)I(MDPP)]$_2$. Similar trends can be noted for $|\vec{r}_{Er-Er}|$
and $\theta_{ErCOT\text{-}r}$. The second factor of interest is of the coordination environment, specifically the hard, anionic alkoxides and $|\vec{r}_{ErCOT}|$. The [Er(COT)]$^+$ unit has demonstrated stability of its single-ion anisotropy in low-symmetry environments with soft Lewis basic ligands, yet the alkoxides represent a significant, localized perturbation to the Er^{3+} free ion spin-orbit ground state. Thus, while in all previous [Er(COT)]$^+$ structures φ_{ligand} has been smaller than the magic angle, the marked increase in Lewis basicity of the alkoxide ligands is expected to more drastically perturb the Er^{3+} J = 15/2 manifold than the weakly Lewis basic iodide ligand. Similarly, $|\vec{r}_{ErCOT}|$ is dramatically shorter at all Er^{3+} centers in **1** and **2** than in complexes we have previously described. We have justified [Er(COT)]$^+$ as a suitable magnetic building block because a single COT^{2-} ligand can reliably stabilize the ground state anisotropy of Er^{3+}. This stabilization decreases as $|\vec{r}_{ErCOT}|$ increases;[45] as we have previously discussed; we therefore expect the single-ion anisotropy of **1** and **2** to weaken compared to our previously described complexes.

We also wish to bring attention to the effect of steric bulk in anionic ligands on the coordination behavior of half-sandwich complexes. As observed with bridging halides, the small ethoxide ligand allows for the formation of an inversion symmetric dinuclear structure. With the increase in bulk in alkoxide bridges comes a large steric demand in the coordination environment. The steric crowding enforces a bent bridging motif, even preventing THF coordination on one Er^{3+} center. In an extreme case of steric bulk, Meng *et al* have used a terphenyl-oxide to isolate a mononuclear [Er(COT)]$^+$ structure.[46]

Table 1: Selected crystallographic and magnetic parameters from **1**, **2**, and previously described [Er(COT)]$^+$ species.

	$\Delta KD_{1\text{-}0}$	g_x	g_y	g_z	θ_{cant}	$\theta_{gz\text{-}r}$	$\theta_{gz\text{-}gz'}$	r_{ErCOT}	Φ_{OR}	$\Phi_{OR'}$	Φ_{THF}
Er-1	53.7 cm^{-1}	0.0289	0.0834	17.4396	2.60°	29.42°	180°	1.82 Å	43.45°	45.56°	54.71°
Er-2a	48.6 cm^{-1}	0.2390	0.1184	17.2907	3.81°	57.74°	109.1°	1.84 Å	49.04°	49.04°	50.00°
Er-2b	34.5 cm^{-1}	0.0033	0.2678	17.0930	9.46°	13.21°		1.79 Å	37.19°	37.19°	–
Er(COT)I-THF$_2$	99.8 cm^{-1}	0.007	0.011	17.820	1.49°	–	–	1.77 Å	49.71° (I)	55.00° (THF)	48.64° (THF)
[Er(COT)I-(MDPP)]$_2$	96.4 cm^{-1}	0.0006	0.0009	17.9051	1.48°	25.99°	180°	1.745 Å	46.62° (I)	47.21° (I)	55.65° (MDPP)

Computational Analysis of Magnetic Anisotropy

A series of *ab initio* calculations were performed to obtain insight into the crystal field perturbations on and differences between the single-ion magnetism of Er^{3+} in Er-**1**, Er-**2a**, and Er-**2b**. Electronic structures for **1** and **2** were modelled with MOLCAS 8.2[47] using complete active space self-consistent field (CASSCF) techniques (Tables 1, S5-S8, Figures S17-S19). Input atom coordinates were taken from crystallographic data without further geometrical optimization. To investigate the single-ion anisotropy of the individual Er^{3+} center, each unique Er^{3+} ion was modelled as the lone magnetic ion by substituting the other erbium center with diamagnetic Y^{3+}, chosen for its similar ionic radius.

The alkoxide bridging motif in **1** and **2** show deviations from previously described [Er(COT)]$^+$ crystal fields in several notable ways. Each center still displays clear ground-state g-factor anisotropy, as expected for an Er^{3+} center bound to COT^{2-} ion; however, the transverse elements (g_x, g_y) for each center are larger than have been previously described, indicating the predicted weakened anisotropy. The first excited Kramers doublet (KD_1) for each Er**1**, **2a**, and **2b** lie 54, 49, and 35 cm^{-1} above the ground state (KD_0), respectively. These splitting are notably smaller than those calculated for previous halide-bound mononuclear and dinuclear [Er(COT)]$^+$ species (U_{eff} > 90 cm^{-1}), indicating that the alkoxides significantly destabilize the single-ion anisotropy in comparison. The barriers are consistent, however, with computed barriers for a recently reported mononuclear phenoxide-bound [Er(COT)]$^+$ complex ($\Delta KD_{1\text{-}0}$ = 55 cm^{-1}).[46] The THF-complexed Er^{3+} centers (Er**1** and Er-**2a**) display a larger $\Delta KD_{1\text{-}0}$ than Er-**2b**, though only on the order of 10 cm^{-1}. Angles between the principle anisotropy axis (g_z) and $\vec{r}_{ErCOT}$, θ_{cant}, have been calculated, and for all three unique Er^{3+} centers the magnetic axis retains a relationship with $\vec{r}_{ErCOT}$, though deviations are larger than previously observed. For comparatively soft Lewis-basic ligands, the COT^{2-} ligand overwhelmingly directs local anisotropy in Er^{3+} half-sandwich coordination environments by stabilizing the prolate high-moment ground spin-orbit state.[31,32] Er**1** and Er-**2a** display deviations of

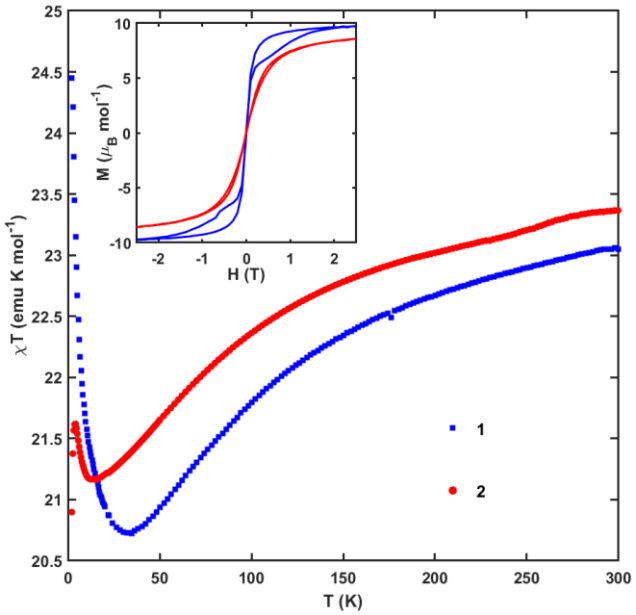

Figure 2: $\chi_M T$ vs. T measurements from 2 to 300 K for **1** (blue squares) and **2** (red circles). (Inset) Isothermal magnetization between -2.5 T and 2.5 T at 2 K for **1** (blue) and **2** (red)

θ_{cant} = 2.6° and 3.8°, while Er-**2b** deviates significantly more with θ_{cant} = 9.5°. This large θ_{cant} for Er-**2b** deviates more dramatically from $\vec{r}_{ErCOT}$ than any mononuclear or dinuclear $[Er(COT)]^+$ species we have previously reported, and those for Er-**1** and Er-**2a** are also comparatively large. Evidently, the $[Er(COT)]^+$ stabilization is heavily strained by the charge density distribution provided by alkoxide ligands at Er^{3+} centers with low symmetry.

Transverse matrix elements connecting the m_J states in the J = 15/2 manifold have been tabulated (Tables S6-8) and plotted for the lowest four m_J states (Figures S15-17). The magnitude of these elements are roughly proportional to their respective transition rates.[48] The rate of excitation to KD_1 is at least ten times faster than the through-barrier relaxation for all centers, indicating that the primary thermally-activated relaxation pathway will involve KD_1 in both **1** and **2**. While the ground spin-orbit states of all three centers display primarily m_J = 15/2 character (~60%), heavy mixing with lower moment states is present. This justifies the relatively large matrix elements between them and indicates a large expected contribution of QTM mechanisms to relaxation dynamics. The first excited state also displays unfavorable mixing, with m_J = 1/2 (28-51%) being the primary contributor for each center. Consequently, matrix elements between the first excited states are on the same order of magnitude as those for excitation to the second excited state for all centers besides Er-**2b**, which displays the smallest degree of m_J = 1/2 contribution to KD_1. The mixing of states in KD_0 is consistent with the non-optimal geometry of $[Er(COT)]^+$ half-sandwich complexes, though the degree of mixing in KD_0 and KD_1 is likely more pronounced due to the stronger crystal field perturbation afforded by the alkoxide ligands.

Lastly, the angle between g_z and $\vec{r}_{Er-Er'}$ ($\theta_{g\text{-}r}$) and the angle between principle anisotropy axes ($\theta_{gz\text{-}gz'}$) were determined as a comparison to the crystallographic parameters described above. For Er**1**, $\theta_{g\text{-}r}$ = 29.4° for both Er^{3+}, related by the crystallographic inversion center, and $\theta_{gz\text{-}gz'}$ = 180°. The principle anisotropy axes are parallel, but noncolinear. These match well with other inversion symmetric $[Er(COT)]^+$ dinuclear structures we have investigated. Complex **2** deviates significantly from previously observed trends, with $\theta_{g\text{-}r}$ = 57.7° for Er-**2a** and $\theta_{g\text{-}r}$ = 13.21° for Er-**2b**, and $\theta_{gz\text{-}gz'}$ = 109.1°. The orientations of the anisotropy axes in **1** suggest that ferromagnetic dipolar interactions may be favorable, whereas in **2**, the angle between the anisotropy axes makes this far less likely.

Static Magnetic Properties

Zero-field cooled magnetic susceptibilities for each compound were collected between 2 and 300 K under a 1000 Oe applied field (Figures 2, S5, S10). At 300 K, experimental $\chi_M T$ values for **1** (23.05 cm^3 K mol^{-1}) and **2** (23.37 cm^3 K mol^{-1}) agree reasonably well with the theoretical value of 22.96 cm^3 K mol^{-1} for two uncoupled Er^{3+} ions (J = 15/2, g = 6/5). Upon cooling, both **1** and **2** display a steady decline in $\chi_M T$, consistent with higher energy m_J states becoming depopulated, before reaching minima of 20.73 cm^3 K mol^{-1} and 21.17 cm^3 K mol^{-1} at 34 K and 12 K respectively. Compound **1** then shows a sharp rise in $\chi_M T$ to 24.45 cm^3 K mol^{-1} at 2 K, while **2** undergoes a similar rise to 21.62 cm^3 K mol^{-1} at 4 K before dropping again to 20.90 cm^3 K mol^{-1} at 2 K. These sharp rises of $\chi_M T$ at low temperature indicate a predominantly ferromagnetic interaction between the Er^{3+} center in each molecule. While uncommon in lanthanide systems overall, this ferromagnetic interaction is consistent with the coupling observed in other $[Er(COT)]^+$ dinuclear magnetic molecules we have previously described.[32,49] Similarly, this coupling is more pronounced in **1**, which has its anisotropy axes oriented parallel to each other.

Isothermal magnetization studies were conducted between 2 and 300 K under DC fields within the range ±7 T. (Figures 2, S5, S10, 30 Oe s^{-1}, VSM). At 2 K, both complexes show typical saturation behavior in the high-field limit (M_{sat} = 9.9 and 9.2 μ_B mol^{-1} for **1** and **2**, respectively). As the field is swept between 7 and −7 T, waist-restricted magnetic hysteresis is observed in both complexes, with neither showing any remnant magnetization on the timescale of this measurement. This "butterfly hysteresis" is commonly attributed to a QTM relaxation pathway, where transitions within the ground Kramers doublet are faster than the measurement timescale. This is consistent with most other mono- and dinuclear $[Er(COT)]^+$ species we have reported, and is indicative that the ferromagnetic coupling between the $[Er(COT)]^+$ units in both complexes is too weak to totally suppress QTM relaxation pathways in Er^{3+} centers with significantly perturbed anisotropy.

Dynamic Magnetic Properties

The relaxation dynamics of **1** and **2** were studied using AC susceptibility measurement techniques (Figures 3, S6-9, S11-14, Tables S1-4). Relaxation times (τ) for both compounds were calculated from frequency dependent AC susceptibilities at different temperatures (H_{DC} = 0 Oe, ν = 1-1000 Hz) by simultaneously fitting the in-phase (χ') and out-of-phase (χ'') components to a generalized Debye equation.[50] Cole-Cole plots of these fitted data form low-eccentricity semicircles, indicating only a single relaxation time for both compounds at each temperature.

Plotting $\ln(\tau)$ against $1/T$ for **1** reveals two distinct regimes: a roughly linear region corresponding to a temperature-dependent relaxation process at higher temperatures (3.5-4 K) and a temperature-independent plateau corresponding to a QTM process below 2.8 K. Fitting these points to a combination of Orbach and QTM mechanisms yielded an effective barrier (U_{eff}) of 34.8 cm^{-1} and an attempt time (τ_0) of $7 \cdot 10^{-10}$ s, consistent with single-molecule relaxation behavior. The U_{eff} value is significantly lower

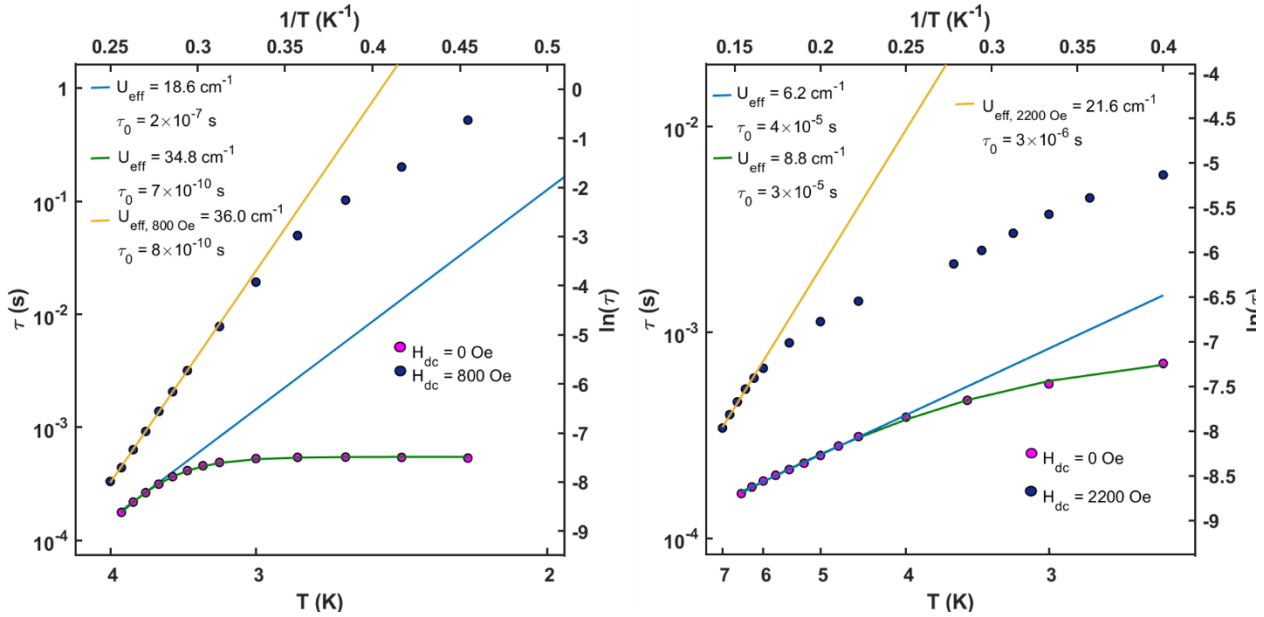

Figure 3: Arrhenius plots of AC magnetometry data for **1** (left) and **2** (right). Zero field data (pink dots) were fit to both an Arrhenius equation at high temperatures (blue lines) and to a combination of Orbach and QTM processes at all temperatures (green curves). Applied field AC susceptibility measurements (navy dots) performed at 800 Oe for **1** and at 2200 Oe for **2** were fit only to an Arrhenius equation at high temperatures (yellow lines)

than the predicted $\Delta KD_{1\text{-}0}$; this discrepancy can be accounted for by the lack of dynamic correlation in the performed calculations and higher degree of covalency between Er^{3+} and COT^{2-} relative to other ligands. A pure Arrhenius linear fitting based on data with $T \geq 3.6$ K yields $U_{eff} = 18.6$ cm^{-1} and $\tau_0 = 2{\cdot}10^{-7}$ s. This behavior is significantly different from dinuclear $[Er(COT)]^+$ species previously described, as the QTM pathways at low temperature are not observably suppressed. The dinuclear $[Er(COT)I(MDPP)]_2$ exhibited long-timescale relaxation, a high barrier above that which was calculated for its individual $[Er(COT)]^+$ centers, and computationally pure ground spin-orbit state; we attributed this to parallel alignment of the Er^{3+} anisotropy axes and weak crystal field perturbations imposed by the soft Lewis basic bridging and ancillary ligands. Contrarily, **1** exhibits fast relaxation, a small barrier below that which was calculated for each center, and a heavily mixed ground and first excited state. Evidently, parallel alignment of $[Er(COT)]^+$ axes is not sufficient to stabilize anisotropy in a dinuclear structure bridged by hard Lewis-basic alkoxide ligands.

The large value for τ_0 measured from the supposed Arrhenius region in **1** indicates that the relaxation mechanism does not proceed predominantly *via* an Orbach mechanism within this temperature range. Thus, AC susceptibility measurements were performed under an optimized 800 Oe applied field to gain a better insight into the Orbach mechanism. The temperature-independent QTM region is no longer apparent above 2 K, and a clear linear region corresponding to a thermally-activated Orbach process in $\ln(\tau)$ vs $1/T$ exists above 3.4 K; fitting an Arrhenius equation to these data yields $U_{eff} = 36.0$ cm^{-1} and $\tau_0 = 8{\cdot}10^{-10}$ s. This barrier corresponds reasonably well with the results obtained from fitting the zero-field AC susceptibility measurements to a combination or Orbach and QTM processes, and the attempt time agrees well with a pure Orbach relaxation mechanism for a lanthanide SMM. Below 3.4 K, the temperature dependence weakens, though relaxation via QTM pathways has been somewhat suppressed.

Surprisingly, the relaxation measurements for **2** revealed a much wider measurable temperature range of relaxation times between 2 and 6.5 K. While $\ln(\tau)$ vs $1/T$ does not clearly level off at low temperatures, indicating that a pure QTM relaxation process is not apparent in the measured temperature range, fitting the data to a combined Orbach and QTM mechanism yields $U_{eff} = 8.8$ cm^{-1} and $\tau_0 = 3{\cdot}10^{-5}$ s. A roughly linear region in $\ln(\tau)$ vs $1/T$ is seen above 4.5 K; an Arrhenius fit of these data gives $U_{eff} = 6.2$ cm^{-1} and $\tau_0 = 4{\cdot}10^{-5}$ s. While this barrier is far smaller than was determined for **1**, relaxation behavior is both seen at higher temperatures and is observed to be slower at 2 K. If we attribute this to the computed single-ion properties, this is consistent with the lower transition probabilities for QTM described for Er-**2b** relative to Er-**1**. The large fitted τ_0 indicate a poorly described Orbach mechanism; thus, AC measurements under an applied DC field were again performed.

AC relaxation measurements were performed under an optimized 2200 Oe applied field. A roughly linear region appears in $\ln(\tau)$ vs $1/T$ above 6.2 K. Fitting this high-temperature linear region to an Arrhenius function between 6.2 K and 7 K yields $U_{eff} = 21.6$ cm^{-1} and $\tau_0 = 2{\cdot}10^{-6}$ s. At lower temperatures, a weaker temperature dependence is observed. This barrier is closer to what is expected computationally, though still deviates significantly. Again, the high τ_0 indicates a poor fit to an Orbach mechanism in the high-temperature regime. As larger applied fields than 2200 Oe do not appreciably change relaxation times for **2**, we were not able to locate a region in which the Orbach mechanism is the dominant relaxation pathway. Therefore, we present $U_{eff} = 21.6$ cm^{-1} as the lower bound for the effective relaxation barrier and $\tau_0 = 2{\cdot}10^{-6}$ as the upper bound for the attempt time.

While calculations show that anisotropy is conserved at each erbium center, both dinuclear complexes were observed to have far lower barriers than were computationally predicted for the single-ion centers and slightly lower barriers than reported for a mononuclear species with one phenoxide ligand ($U_{eff} = 44.1$ cm^{-1}, $H_{DC} = 2500$ Oe).[46] While the $[Er(COT)]^+$ units in **1** are oriented parallel to each other, **2** relaxes almost ten times slower than **1** at 2 K under zero applied field, contrary to the trend we have previously reported for a phosphine-scaffolded iodide-bridged system. This is indicative of a common problem among coupled lanthanide SMMs, wherein it is difficult to balance a favorable coordination environment, suitably strong coupling, and anisotropic alignment of subunits within a cluster. We primarily attribute the differences between **1** and **2** to the surprisingly favorable

relaxation probabilities predicted for Er-**2b**, though the presence of ferromagnetic coupling in both samples complicates the attribution of a clear cause for the discrepancies.

Conclusions

We have synthesized two dinuclear alkoxide bridged single-molecule magnets and described their magnetic properties through comparison of their coordination environment, *ab initio* calculated electronic structure, and static and dynamic magnetic behavior. Both compounds' relaxation behaviors deviate significantly from those previously described for dinuclear $[Er(COT)]^+$ compounds, illustrating the effects of a much stronger crystal field contributed by the hard Lewis basic alkoxide ligands. While the symmetry and angle between the calculated anisotropy axes differ greatly between **1** and **2**, their effective barriers differ very little. Despite the parallel alignment of both metal centers' anisotropy axes, **1** displays a larger QTM contribution to relaxation than **2** and relaxes much more quickly. However, at high temperatures a nearly pure Orbach mechanism can be observed to dictate relaxation under an applied field in **1**, whereas **2** displays multiple operant relaxation processes at all measured temperatures. Though ferromagnetic coupling interactions are clearly present in both systems, single-ion crystal field effects appear to dominate contributions to relaxation behavior at all measured temperatures. From these data, we can refine the design principles toward incorporating the $[Er(COT)]^+$ unit into larger structures. First and foremost, ligands must be judiciously chosen to avoid dramatic perturbation of the anisotropy by hard Lewis basic interactions in an unoptimized geometry. Furthermore, while the orientation of anisotropy axes can enhance coupling between highly anisotropic centers, it is not in and of itself able to overcome poor anisotropy and weak single-ion magnetism. We anticipate that the magnetostructural and synthetic principles gleaned from this study will further facilitate the rational incorporation of anisotropic structural units into complex molecule-based magnets.

ASSOCIATED CONTENT

The Supporting Information is available free of charge on at DOI:

Experimental procedures and physical and computational data for all new compounds, including Figures S1-S17 and Tables S1-S8.

AUTHOR INFORMATION

Corresponding Author

* jrinehart@ucsd.edu

Author Contributions

All authors have given approval to the final version of the manuscript.

Notes

The authors declare no competing financial interest.

ACKNOWLEDGMENTS

This research was funded through the Office of Naval Research, Young Investigator Award N00014-16-1-2917. We thank Drs. Milan Gembicky, Curtis Moore, and Arnold Rheingold for assistance with crystal structure determination.

ABBREVIATIONS

COT, Cyclooctatetraene dianion; O^{t}Bu, *tert*-butoxide; OEt, ethoxide; QTM, Quantum Tunneling of the Magnetization; CASSCF, Complete Active Space Self-Consistent Field; SMM, Single-molecule magnet;

REFERENCES

(1) Sessoli, R.; Gatteschi, D.; Caneschi, A.; Novak, M. A. Magnetic Bistability in a Metal-Ion Cluster. *Nature* **1993,** *365* (6442), 141–143.
(2) Sessoli, R.; Tsai, H. L.; Schake, A. R.; Wang, S.; Vincent, J. B.; Folting, K.; Gatteschi, D.; Christou, G.; Hendrickson, D. N. High-spin molecules: [Mn12O12(O2CR)16(H2O)4] *J. Am. Chem. Soc.* **1993**, *1155*, 1804-1816
(3) Pedersen, K. S.; Bendix, J.; Clérac, R. Single-Molecule Magnet Engineering: Building-Block Approaches. *Chem. Commun*. **2014**, *50* (34), 4396–4415.
(4) Frost, J. M.; Harriman, K. L. M.; Murugesu, M. The Rise of 3-d Single-Ion Magnets in Molecular Magnetism: Towards Materials from Molecules? *Chem. Sci.* **2016**, *7* (4), 2470–2491.
(5) Maniaki, D.; Pilichos, E.; Perlepes, S. P. Coordination Clusters of 3d-Metals That Behave as Single-Molecule Magnets (SMMs): Synthetic Routes and Strategies. *Frontiers in Chemistry.* **2018**, *6*, 461.
(6) Sievers, J. Asphericity of 4f-Shells in Their Hund's Rule Ground States. *Zeitschrift für Physik B Condensed Matter.* **1982**, *45* (4), 289–296.
(7) Rinehart, J. D.; Long, J. R. Exploiting Single-Ion Anisotropy in the Design of f-Element Single-Molecule Magnets. *Chem. Sci.* **2011**, *2* (11), 2078–2085.
(8) McAdams, S. G.; Ariciu, A.-M.; Kostopoulos, A. K.; Walsh, J. P. S.; Tuna, F. Molecular Single-Ion Magnets Based on Lanthanides and Actinides: Design Considerations and New Advances in the Context of Quantum Technologies. *Coordination Chemistry Reviews.* **2017**, *346*, 216–239.
(9) Harriman, K. L. M.; Errulat, D.; Murugesu, M. Magnetic Axiality: Design Principles from Molecules to Materials. *Trends in Chemistry.* **2019**.
(10) Liu, J.-L.; Chen, Y.-C.; Tong, M.-L. Symmetry Strategies for High Performance Lanthanide-Based Single-Molecule Magnets. *Chem. Soc. Rev.* **2018**, *47* (7), 2431–2453.
(11) Dey, A.; Kalita, P.; Chandrasekhar, V. Lanthanide(III)-Based Single-Ion Magnets. *ACS Omega*. **2018**, *3* (8), 9462–9475.

(12) Guo, F.-S.; Day, B. M.; Chen, Y.-C.; Tong, M.-L.; Mansikkamäki, A.; Layfield, R. A. A Dysprosium Metallocene Single-Molecule Magnet Functioning at the Axial Limit. *Angew. Chem., Int. Ed.* **2017**, *56* (38), 11445–11449.
(13) Goodwin, C. A. P.; Ortu, F.; Reta, D.; Chilton, N. F.; Mills, D. P. Molecular Magnetic Hysteresis at 60 Kelvin in Dysprosocenium. *Nature.* **2017**, *548*, 439.
(14) Guo, F.-S.; Day, B. M.; Chen, Y.-C.; Tong, M.-L.; Mansikkamäki, A.; Layfield, R. A. Magnetic Hysteresis up to 80 Kelvin in a Dysprosium Metallocene Single-Molecule Magnet. *Science.* **2018**, *362* (6421), 1400.
(15) Gi ansiracusa, M. J.; Moreno-Pineda, E.; Hussain, R.; Marx, R.; Martínez Prada, M.; Neugebauer, P.; Al-Badran, S.; Collison, D.; Tuna, F.; van Slageren, J.; et al. Measurement of Magnetic Exchange in Asymmetric Lanthanide Dimetallics: Toward a Transferable Theoretical Framework. *J. Am. Chem. Soc.* **2018**, *140* (7), 2504–2513.
(16) Rinehart, J. D.; Fang, M.; Evans, W. J.; Long, J. R. A N23– Radical-Bridged Terbium Complex Exhibiting Magnetic Hysteresis at 14 K. *J. Am. Chem. Soc.* **2011**, *133* (36), 14236–14239.
(17) Demir, S.; Zadrozny, J. M.; Nippe, M.; Long, J. R. Exchange Coupling and Magnetic Blocking in Bipyrimidyl Radical-Bridged Dilanthanide Complexes. *J. Am. Chem. Soc.* **2012**, *134* (45), 18546–18549
(18) Gould, C. A.; Darago, L. E.; Gonzalez, M. I.; Demir, S.; Long, J. R. A Trinuclear Radical-Bridged Lanthanide Single-Molecule Magnet. *Angew. Chem., Int. Ed.* **2017**, *56* (34), 10103–10107.
(19) Steenbock, T.; Shultz, D. A.; Kirk, M. L.; Herrmann, C. Influence of Radical Bridges on Electron Spin Coupling. *J. Phys. Chem. A.* **2017**, *121* (1), 216–225.
(20) Huang, G.; Daiguebonne, C.; Calvez, G.; Suffren, Y.; Guillou, O.; Guizouarn, T.; Le Guennic, B.; Cador, O.; Bernot, K. Strong Magnetic Coupling and Single-Molecule-Magnet Behavior in Lanthanide-TEMPO Radical Chains. *Inorg. Chem.* **2018**, *57* (17), 11044–11057.
(21) Le Roy, J. J.; Jeletic, M.; Gorelsky, S. I.; Korobkov, I.; Ungur, L.; Chibotaru, L. F.; Murugesu, M. An Organometallic Building Block Approach To Produce a Multidecker 4f Single-Molecule Magnet. *J. Am. Chem. Soc.* **2013**, *135* (9), 3502–3510.
(22) Harriman, K. L. M.; Murugesu, M. An Organolanthanide Building Block Approach to Single-Molecule Magnets. *Acc. Chem. Res.* **2016**, *49* (6),
(23) Jiang, S.-D.; Wang, B.-W.; Sun, H.-L.; Wang, Z.-M.; Gao, S. An Organometallic Single-Ion Magnet. *J. Am. Chem. Soc.* **2011**, *133* (13), 4730–4733.
(24) Jiang, S.-D.; Liu, S.-S.; Zhou, L.-N.; Wang, B.-W.; Wang, Z.-M.; Gao, S. Series of Lanthanide Organometallic Single-Ion Magnets. *Inorg. Chem.* **2012**, *51* (5), 3079–3087.
(25) Meihaus, K. R.; Long, J. R. Magnetic Blocking at 10 K and a Dipolar-Mediated Avalanche in Salts of the Bis(H8-Cyclooctatetraenide) Complex [Er(COT)2]−. *J. Am. Chem. Soc.* **2013**, *135* (47), 17952–17957.
(26) Le Roy, J. J.; Korobkov, I.; Murugesu, M. A Sandwich Complex with Axial Symmetry for Harnessing the Anisotropy in a Prolate Erbium(III) Ion. *Chem. Commun.* **2014**, *50* (13), 1602–1604.
(27) Le Roy, J. J.; Ungur, L.; Korobkov, I.; Chibotaru, L. F.; Murugesu, M. Coupling Strategies to Enhance Single-Molecule Magnet Properties of Erbium–Cyclooctatetraenyl Complexes. *J. Am. Chem. Soc.* **2014**, *136* (22), 8003–8010.
(28) Ungur, L.; Le Roy, J. J.; Korobkov, I.; Murugesu, M.; Chibotaru, L. F. Fine-Tuning the Local Symmetry to Attain Record Blocking Temperature and Magnetic Remanence in a Single-Ion Magnet. *Angew. Chem. Int. Ed.* **2014**, *126* (17), 4502–4506.
(29) Meng, Y.-S.; Wang, C.-H.; Zhang, Y.-Q.; Leng, X.-B.; Wang, B.-W.; Chen, Y.-F.; Gao, S. (Boratabenzene)(Cyclooctatetraenyl) Lanthanide Complexes: A New Type of Organometallic Single-Ion Magnet. *Inorg. Chem. Front.* **2016**, *3* (6), 828–835.
(30) He, M.; Chen, X.; Bodenstein, T.; Nyvang, A.; Schmidt, S. F. M.; Peng, Y.; Moreno-Pineda, E.; Ruben, M.; Fink, K.; Gamer, M. T.; et al. Enantiopure Benzamidinate/Cyclooctatetraene Complexes of the Rare-Earth Elements: Synthesis, Structure, and Magnetism. *Organometallics* **2018**, *37* (21), 3708–3717.
(31) Hilgar, J. D.; Bernbeck, M. G.; Flores, B. S.; Rinehart, J. D. Metal–Ligand Pair Anisotropy in a Series of Mononuclear Er–COT Complexes. *Chem. Sci.* **2018**, *9* (36), 7204–7209.
(32) Hilgar, J. D.; Bernbeck, M. G.; Rinehart, J. D. Million-Fold Relaxation Time Enhancement across a Series of Phosphino-Supported Erbium Single-Molecule Magnets. *J. Am. Chem. Soc.* **2019**, *141* (5), 1913–1917.
(33) Westin, L. G.; Kritikos, M.; Caneschi, A. Self Assembly, Structure and Properties of the Decanuclear Lanthanide Ring Complex, Dy10(OC2H4OCH3)30. *Chem. Commun.* **2003**, *0* (8), 1012–1013.
(34) Yang, P.-P.; Gao, X.-F.; Song, H.-B.; Zhang, S.; Mei, X.-L.; Li, L.-C.; Liao, D.-Z. Slow Magnetic Relaxation in Novel Dy4 and Dy8 Compounds. *Inorg. Chem.* **2011**, *50* (3), 720–722.
(35) Baniodeh, A.; Magnani, N.; Bräse, S.; Anson, C. E.; Powell, A. K. Ligand Field Variations: Tuning the Toroidal Moment of Dy6 Rings. *Dalton Trans.* **2015**, *44* (14), 6343–6347.
(36) Gao, F.; Feng, X.; Yang, L.; Chen, X. New Sandwich-Type Lanthanide Complexes Based on Closed-Macrocyclic Schiff Base and Phthalocyanine Molecules. *Dalton Trans.* **2016**, *45* (17), 7476–7482.
(37) Sun, H.; Liu, M.; Zhang, B. Two Dysprosium Complexes Based on 8-Hydroxyquinoline Schiff Base: Structures, Luminescence Properties and Single-Molecule Magnets Behaviors. *Inorganica Chimica Acta*. **2016**, *453*, 681–686.
(38) Peng, G.; Zhang, Y.-Y.; Li, Z.-Y.; Kostakis, G. E. First Examples of Polynuclear Lanthanide Diethylene Glycol Based Coordination Clusters. *Eur. J. Inorg. Chem.* **2017**, *2017* (20), 2700–2706.
(39) Baniodeh, A.; Mondal, A.; Galeev, R.; Sukhanov, A.; Eremina, R.; Voronkova, V.; Anson, C. E.; Powell, A. K. How Far Can the Anisotropy Deviate from Uniaxiality in a Dy-Based Single-Molecule Magnet? Dinuclear Dy(III) Complex Study. *Appl. Magn. Reson.* **2017**, *48* (1), 101–113.
(40) Zahra, A.; Mahmud, T.; Tahir, M. N.; Shad, H. A.; Rehman, H.; Naseem, S. Synthesis, Characterization and Magnetic Studies of Dysprosium Complex, [Dy2(TEA)2(O2CPh)4·2H2O]. *J. Chem. Crystallogr.* **2017**, *47* (5), 151–156.
(41) Wang, W.-M.; Wang, S.; Wu, Z.-L.; Ran, Y.-G.; Ren, Y.-H.; Zhang, C.-F.; Fang, M. Two Phenoxo-O Bridged Dy2 Complexes Based on 8-Hydroxyquinolin Derivatives with Different Magnetic Relaxation Features. *Inorg. Chem. Commun.* **2017**, *76*, 48–51.
(42) Palumbo, C. T.; Darago, L. E.; Windorff, C. J.; Ziller, J. W.; Evans, W. J. Trimethylsilyl versus Bis(Trimethylsilyl) Substitution in Tris(Cyclopentadienyl) Complexes of La, Ce, and Pr: Comparison of Structure, Magnetic Properties, and Reactivity. *Organometallics.* **2018**, *37* (6), 900–905.
(43) Guo, Y.-N.; Xu, G.-F.; Wernsdorfer, W.; Ungur, L.; Guo, Y.; Tang, J.; Zhang, H.-J.; Chibotaru, L. F.; Powell, A. K. Strong Axiality and Ising Exchange Interaction Suppress Zero-Field Tunneling of Magnetization of an Asymmetric Dy2 Single-Molecule Magnet. *J. Am. Chem. Soc.* **2011**, *133* (31), 11948–11951.
(44) Cendrowski-Guillaume, S. M.; Le Gland, G.; Nierlich, M.; Ephritikhine, M. Lanthanide Borohydrides as Precursors to Organometallic Compounds. Mono(Cyclooctatetraenyl) Neodymium Complexes. *Organometallics.* **2000**, *19* (26), 5654–5660.

(45) Chen, S.-M.; Xiong, J.; Zhang, Y.-Q.; Yuan, Q.; Wang, B.-W.; Gao, S. A Soft Phosphorus Atom to "Harden" an Erbium(III) Single-Ion Magnet. *Chem. Sci.* **2018**, *9* (38), 7540–7545.
(46) Meng, Y.-S.; Yang, M.-W.; Xu, L.; Xiong, J.; Hu, J.-Y.; Liu, T.; Wang, B.-W.; Gao, S. Design Principle of Half-Sandwich Type Erbium Single-Ion Magnets through Crystal Field Engineering: A Combined Magnetic and Electronic Structure Study. *Dalton Trans.* **2019**, Advance Article.
(47) Aquilante, F.; Autschbach, J.; Carlson, R. K.; Chibotaru, L. F.; Delcey, M. G.; De Vico, L.; Galvan, I. F.; Ferre´, N.; Frutos, L. M.;´ Gagliardi, L.; Garavelli, M.; Giussani, A.; Hoyer, C. E.; Le Manni, G.; Lischka, H.; Ma, D.; Malmqvist, P. A.; Müller, T.; Nenov, A.; Olivucci, M.; Pedersen, T. B.; Peng, D.; Plasser, F.; Pritchard, B.; Reiher, M.; Rivalta, I.; Schapiro, I.; Segarra-Martí, J.; Stenrup, M.; Truhlar, D. G.; Ungur, L.; Valentini, A.; Vancoillie, S.; Veryazov, V.; Vysotskiy, V. P.; Weingart, O.; Zapata, F.; Lindh, R. Molcas 8: New Capabilities for Multiconfigurational Quantum Chemical Calculations across the Periodic Table. *J. Comput. Chem.* **2016**, *37*, 506–541
(48) Ungur, L.; Chibotaru, L. F. Magnetic Anisotropy in the Excited States of Low Symmetry Lanthanide Complexes. *Phys. Chem. Chem. Phys*. **2011**, *13* (45), 20086–20090
(49) Hilgar, J. D.; Flores, B. S.; Rinehart, J. D. Ferromagnetic Coupling in a Chloride-Bridged Erbium Single-Molecule Magnet. *Chem. Commun.* **2017**, *53* (53), 7322–7324.
(50) Gatteschi, D.; Sessoli, R.; Villain, J. *Molecular Nanomagnets*; 2006; Vol. 376.

Graphical TOC Entry